Morphology-Property Relationship in Radially Oriented Anchored Carbon Nanotubes on Polybenzimidazole Nanofibers

Kaan Yildiz,[a,b] Adel Alrai,[b,c], Melike Erturk,[b,c] Deniz Koken,[d,e] Beyza Bozali,[b] Afshin Zamani Zakaria,[f] Fevzi Cakmak Cebeci,[d,e] Elif Ozden-Yenigun,[g,*] and Hulya Cebeci[b,c,*]

[a] Aviation Institute, Istanbul Technical University, 34467, Istanbul, Turkey.
[b] Aerospace Research Center, Istanbul Technical University, 34467, Istanbul, Turkey.
[c] Faculty of Aeronautics and Astronautics, Istanbul Technical University, 34467, Istanbul, Turkey.
[d] Faculty of Engineering and Natural Sciences, Sabanci University, 34956, Istanbul, Turkey.
[e] Sabanci University SUNUM Nanotechnology Research Center, 34956, Istanbul Turkey.
[f] School of Environment and Science, Griffith University, Brisbane, Queensland 4111, Australia.
[g] School of Design, Textiles, Royal College of Art, SW7 2EU, London, United Kingdom.

Abstract: Introducing carbon nanotubes (CNTs) with the capability of anchoring on nanofibers establishes new possibilities in many applications such as lithium-sulphur batteries and laminated composites. Direct growth and attachment of CNTs eliminate dispersion challenges such as detachment or transfer of CNTs onto another medium and damage on CNTs, leading to inadequacy for practical applications. This study facilitated the direct growth of conductive CNTs on curved, high-temperature resistant polymeric polybenzimidazole (PBI) nanofibers by chemical vapor deposition method (CVD). Controlling CVD process parameters including nucleation and growth times (10 or 15 minutes) and catalyst concentration (1 or 10 mM) at 600 °C facilitated the growth of radially-oriented CNTs on PBI nanofibers and provided morphology-dominated behavior both on physical and electrical properties. Morphological analyses showed that tuning catalyst concentration (10 mM) and CVD process parameters including nucleation (15 min) and growth times (10 min and 15 min) yielded uniform CNT coverage and conformity. A systematic exploration of mesoscopic morphologies revealed a strong correlation between physical parameters such as CNT array lengths and electrical conductivity which is up to 0.039±0.004 S/cm. The proposed CNT growth method could offer in-situ structural tunability to respond to application-related requirements from energy storage to the rate capability of lithium-based batteries.

Keywords: nanofibers; carbon nanotubes; chemical vapor deposition; polybenzimidazole

* Corresponding authors. E-mail address: elif.ozden-yenigun@rca.ac.uk (Elif Ozden-Yenigun); hulya.cebeci@itu.edu.tr (Hulya Cebeci).

1. Introduction

Carbon nanotubes (CNTs) incorporated material systems have been one of the well-known lightweight solutions to a wide range of applications ranging from energy storage and interface reinforcement in laminated composites to the life cycle and rate capability booster in lithium-ion capacitors and lithium-sulfur batteries [1–7]. Opposed to commonly adopted approaches of dispersing and distributing CNTs into a polymer medium [8–10] or surface coating techniques [11], direct deposition of CNTs onto the surface of a substrate has found a novel and promising role in hierarchical composites [12] and conductive micro-devices [13]. Promoted by the superior electrical conductivity properties of CNTs, the capacity and the efficiency of rechargeable lithium batteries could be enhanced by placing CNT-based interleaves between the separator and the sulfur cathode. Furthermore, the delamination that afflicts the durability in laminated composite structures could be prevented by distinct CNT-based interfaces which enhances fracture toughness and high delamination resistance [14–17]. Thus, the growth of CNTs onto distinct substrates and their controlled architectures enable keeping the CNTs intact; therefore, significant attention has been given to the CNTs direct growth procedures along with process optimization [18–20].

CNT hierarchical composites are found in various applications such as energy storage and harvesting units, air filtration, and reinforced structural composites. CNT grafted hybrid fabrics with high surface area and electrical conductivity were shown to have a potential to be implemented as electrodes for the production of flexible supercapacitors [21]. Additionally, lithium-CNT microsphere composites as electrodes in lithium-based batteries were proven to be a solution to prevent dendrite formation on the surface of electrodes, thus, increasing recharging cycles [22]. In another study, $ZnMn_2O_4$-CNT composites were used as a cathode material for zinc-ion batteries with high specific capacity (mAh/g) [23]. Recently, a polyvinylidene fluoride (PVDF) CNT foam composite nanogenerator was shown to not only exhibit good flexibility but also high piezoelectric performance with an output voltage of 15 V under a compressive force [24]. Furthermore, CNTs incorporated in fibrous membrane used for air filtration applications provided high porosity, leading to low-pressure drop and high capturing capacity [25]. Other studies also reported CNT-incorporated nanofibrous interlayers as functional interlaminar reinforcements [26–29].

Regardless of the orientation in CNT growth, to implement CNTs in later processes, the grown-CNTs usually are peeled off or transferred onto another medium. As a result of this post step, the CNTs

could be severely damaged, making them inadequate for sensory applications. As an alternative to conventional film-based substrates, nanofiber scaffolds as interleaves are beneficial as a result of their interconnected porous structure and high surface area [30]. Additionally, direct deposition of CNTs onto either nano- or micro-scale fibers have the potential of using these strong and conductive reinforcers without tarnishing the quality of the CNTs or adding post-processes such as the collection, dispersion, and distribution steps. Although this approach promotes fewer steps, the substrate on which CNTs grow need to stay intact at the elevated synthesis temperature. Hence, it is vital that the polymeric substrate withstands high temperatures during CNT synthesis.

Poly[2,2'-(m-phenylene)-5,5'-bibenzimidazole], also known as polybenzimidazole (PBI) is a heat resistant and high-performance polymer that exhibits remarkable chemical resistance, high thermal and oxidative stability [31]. PBI nanofibrous scaffolds have received attention due to their high surface area, porous and interconnected structure in many applications from the high-temperature fuel cell and reverse osmosis, gas separation systems, to interface toughening in laminated composites, and etc. [32,33]. First, Kim and Reneker explored the electrospinning of PBI nanofibers [34], by emphasizing on the increase in Young's modulus and fracture toughness, as a reinforcement [35]. Apart from their use in composites, the high-performance capabilities of PBI nanofibers have also been reported as a successful membrane proton exchange membrane (PEM) material in fuel cells [33,36]. Doped by phosphoric acid, crosslinked PBI nanofibers enhanced PEM fuel cell performance along with increased proton conductivity and mechanical properties [37].

Among many methods for the synthesis of CNTs, chemical vapor deposition (CVD) has come forward as one of the most efficient methods due to its versatility to work with different substrates and catalyst types, ease of scaling, high-yield CNT production, and controllability of the alignment [29,38]. Physical properties of CNTs such as orientation, array density, and length could be tuned by CVD process parameters such as growth and nucleation times [8,18,39,40], the flow rate of gases [41], growth temperature [41,42], and catalyst concentration [12,40]. Agnihotri et al. studied the effect of growth time on the density and length of grown-CNTs on carbon fibers and concluded that CNTs could lose their orientation with over-growth [19]. In another study, Singh et al. highlighted that the high degree of alignment in CNTs anchored onto the micron-sized fibers was due to the resulting crowding effect (steric hindrance) between nanotubes, while low catalyst density caused random orientation of CNTs [43]. Setting growth temperature lower than the carbon-iron eutectic temperature, 723 °C,

randomly oriented CNTs were produced, associated with low solubility of carbon in the iron catalyst. Beyond this temperature, however, gas kinetics promoted controlled deposition of stable CNTs onto the fiber surfaces [12].

It is important to note that the CNT alignment is not affected only by the process parameters, but also by the texture and morphology of the base substrate. In particular applications, e.g. sensors, control of orientation is essential for electron transport [44]. Thus, in such structural restraints, the most critical parameters affecting the orientation of CNTs were reported to be the crystallographic orientation of the substrate, density of the nucleation sites and size of the isolated catalyst particles [38]. Handuja et.al. reported well-aligned and uniform CNT growth on an untreated and Fe-deposited quartz substrate, while a copper substrate did not work as a convenient medium for the growth that encouraged the agglomerated amorphous phase on the surface [45]. From this perspective, silica-based substrates work more efficiently than quartz substrates in which higher CNT density and densely ordered CNT structure were achieved owing to existing repulsion forces among the adjacent CNTs [46]. Vertically aligned CNTs (CNT forest or arrays) have been successfully grown on different smooth substrates depending on systematic control on growth conditions and catalyst amount [47]. The separation distance between accumulated catalysts nanoparticles on substrate surface affected the self-assembly ability of CNTs. Xu et al. successfully tailored the active catalyst formation during the growth stage, by monitoring CNT alignment depending on catalyst density in which crowding effect between neighboring CNTs was observed with an increase in density [48]. However, to what extent the nanoscopic features of a polymeric substrate could affect the control of CNT architectures and, subsequently, electrical, and thermal and mechanical properties of the nanocomposite is yet to be studied.

To the best of our knowledge, the synergetic effect of both oriented CNTs and nanofibrous networks, which could open up new possibilities in nano-engineered polymer composites, is not completely addressed by researchers. This manuscript systematically attempts to reveal how we could benefit from the intrinsic merits of nanofibrous substrates by controlling CNTs orientation on nanofibers.

This study tackles material-based challenges such as thermal degradation in polymer nanofibers and control of CNT orientation on heterogenous rough nanofibrous mediums. The experimental methodology began with the optimization of the CVD process to grow radially oriented CNTs on

electrospun PBI nanofibers, referred to as nanocarpets. PBI nanofibrous scaffold provided remarkably high surface area and well-connected porous network for CNT growth in which the intrinsic properties such as degradation temperature restrained growth process. After a series of process optimization in PBI nanofiber production based on monitoring the surface irregularities and fiber diameter changes, these nanofibrous scaffolds were utilized as the base for CNT growth where the process parameters were systematically regulated. This study intends to reveal the range of material quantities such as CNT physical parameters, coverage and density of CNTs and the CNT quality that could be tuned by the control of CVD process parameters coupled with nanofibrous surfaces. Transmission electron microscopy (TEM) images revealed that radially anchored CNTs could be grown onto 100 µm thick PBI nanofibers, with the I_g/I_d ratio of ~1.11 and the electrical conductivity in the range of 0.004 and 0.039 S/cm.

2. Materials and Methods

2.1 Materials

PBI (Poly[2,2'-(m-phenylene)-5,5'-bibenzimidazole]) S26 solution with a viscosity of 2100±200 Poise at 25 °C (containing 26.2 weight percent (wt.%) PBI powder with molecular weight of 308 g/mole, 72.3 wt.% N, N-dimethylacetamide (DMAc) and 1.5 wt.% LiCl) was purchased from PBI Performance Products, Inc. (USA). PBI solution was first diluted to 20 wt.% using DMAc, supplied by Sigma-Aldrich, to form the solution to be used in electrospinning. The solution was stirred magnetically at 150 rpm for 24 hours (h) and later kept in an oil bath for 2 h at 50 °C to ensure homogenization. For the reproducibility concerns, all the following preparation processes and characterization were repeated at least five times.

2.2 Preparation of PBI Nanofibers

PBI nanofibers were produced by an electrospinning device (Argeteknolab), which consists of a pump system (NewEra NE 1000 Syringe Pump) with a 5 ml syringe, a high voltage generator, and a rotary collector. During the electrospinning process, a 20 kV electrical potential was applied to the needle (inner diameter of 300 µm) while the distance between the needle tip and the collector was 15 cm and the flow rate of the polymer solution was kept constant at 150 µl/h by the syringe pump. Polymer solutions were prepared by dissolving 20 wt.% PBI. After two hours of electrospinning, 100-micron thick nanofibers were deposited and collected for further CVD processes.

2.3 Process of Catalysis

Nanofibrous mats cut into 2×5 cm^2 were catalyzed by using a spin coater at 500 rpm for 5 minutes (min). At two different concentrations, 1 mM and 10 mM of $Fe(NO_3)_3 \cdot 9H_2O$ (purchased from Emir Kimya) precursors were dissolved in isopropyl alcohol (Sigma Aldrich) and later used as the catalyst solution. Deposited Fe^{3+} ions onto nanofibers served as the nucleation sites for CNT growth. After the catalysis process, these nanofibrous mats were desiccated at 50 °C for 5 h in an oven. The scanning electron microscopy (SEM) image of the accumulated Fe^{3+} particles using 10 mM catalyst solution on PBI nanofibers and the particle size distribution are shown in the Supplementary Information (Fig. S1).

2.4 Synthesis of CNTs Grown PBI Nanocarpets

Catalyst deposited nanofibrous mats were placed in the quartz tube for the CVD process. Before the nucleation stage, helium gas was purged in with a flow rate of 1000 standard cubic centimeters per minute (sccm) to the quartz tube of the CVD furnace (Lindberg Blue/M) to provide an inert environment for the growth procedure (Fig. 1) while heating the oven simultaneously (0-t_1). During the nucleation stage (t_1-t_2), helium and hydrogen gases were flushed in with flow rates of 1600 sccm and 1000 sccm, respectively, to create nucleation sites. Then, in the growth stage (t_2-t_3), the flow rates of helium (He) and hydrogen (H_2) gases were reduced to 1000 sccm and 600 sccm, respectively, and the carbon source gas (C_2H_4) was introduced with a flow rate of 400 sccm to the system to facilitate CNT growth. Finally, the furnace was cooled down to room temperature under the He flushing with a flow rate of 300 sccm after the CNT growth was terminated. All the process gases were purchased from Air Liquide, Turkey.

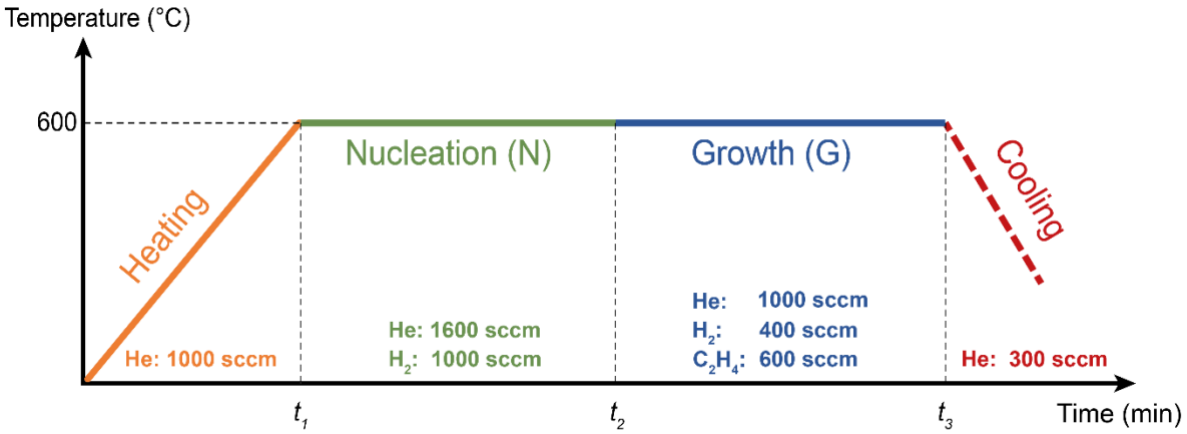

Fig. 1 A representation of CVD time-temperature profile performed for CNT growth presenting 0-t_1 as heating, t_1-t_2 as nucleating, t_2-t_3 as growth and over t_3 as cooling time in minutes.

2.5 Characterization

The morphologies of both PBI nanocarpets and CNT anchored nanocarpets were characterized using various magnification by a QUANTA FEG SEM at 15 kV. TGA analysis was conducted using TA Instruments (SDT Q600) with a flow rate of 100 ml/min under N_2 atmosphere to investigate the thermal stability of neat PBI nanofibers. Moreover, individual nanofibers were isolated by immersing in ethanol solvent using an ultrasonic cleaner for 10 min to retrieve the structural information of individual CNTs. Then, these small chunks of fibers were placed onto the grid surface (EMS CF200-Cu) under an optical microscope. The prepared grids were investigated using JEOL 2100 HRTEM (200 kV) by zooming in individual CNTs on PBI nanofiber. Raman spectroscopy was conducted using Renishaw inVia reflex microscopy with an excitation energy of 2.32 eV and acquisition in the range of 100-3000 cm^{-1}. The green laser (λ=532 nm) was used for Raman analysis, and all CNTs/PBI nanocarpets were mapped in 40×40 micron-squared to determine the quality of CNTs. Electrical conductivity measurements were carried out by a four-point probe with a surface probe (FPP-470A, Entek Elektronik).

3. Results and Discussion

3.1 Electrospun PBI Nanofibrous Scaffolds

The electrospinning method facilitated the production of PBI nanofibrous substrates with high porosity and surface area. Fig. 2a-b show the randomly oriented as-prepared PBI nanofibers and the histogram of the mean fiber diameter, respectively. The mean fiber diameter of PBI nanofibers was calculated as 408±41 nm. Further, Fig. 2a reveals the high porosity of the structure, which favors interfacial adhesion to adjacent plies and better bonding, particularly in interlaminar reinforcement [49]. Using a publicly available MATLAB code, the SEM image given in Fig. 2a was analyzed to quantify the porosity of the neat nanofibers (Fig. S2). As a result of the analyses, the porosity of the neat nanofibers was found to be approximately 20% [50,51].

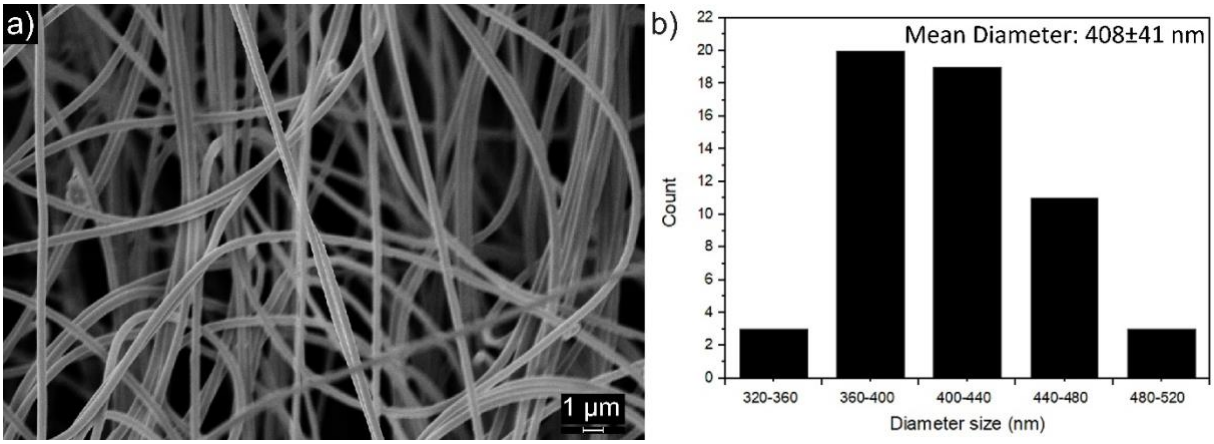

Fig. 2 a) Randomly oriented electrospun PBI nanofibers, as later used as the base in CNT growth and b) the mean fiber diameter distribution of PBI nanofibers.

The thermogravimetric analysis was conducted to understand the thermal stability and mass changes for the upcoming CVD process to synthesize CNTs. Fig. 3a reveals that the first mass change interpreted from DTG (%/°C) took place around 80 °C due to the decomposition of the LiCl stabilizer [52]. CNT growth and nucleation temperatures in the CVD method could be tuned in a way not to exceed the PBI decomposition range, which was determined to be around 700 °C in compliance with earlier studies [33]. Exceeding this temperature caused the decomposition of the polymer backbone, which can be traced by the notable weight loss shown in Fig. 3a [53]. Hence, the stability of the PBI nanofibers were investigated at 600 °C for the weight loss. CVD protocol to heat the PBI nanofibers was applied up to 600 °C and then followed by a TGA analysis to determine the thermal stability. The results revealed that the weight loss of neat and heat-treated PBI nanofibers at 600 °C are approximately 25% and 10%, respectively, as demonstrated in Fig. 3a and 3b. The increase in the thermal stability with heat-treatment at 600 °C confirms the usability of PBI nanofibers for CNT synthesis. Based on the results and considering the required high temperatures to activate the catalyst, the CVD growth temperature was determined to be 600 °C.

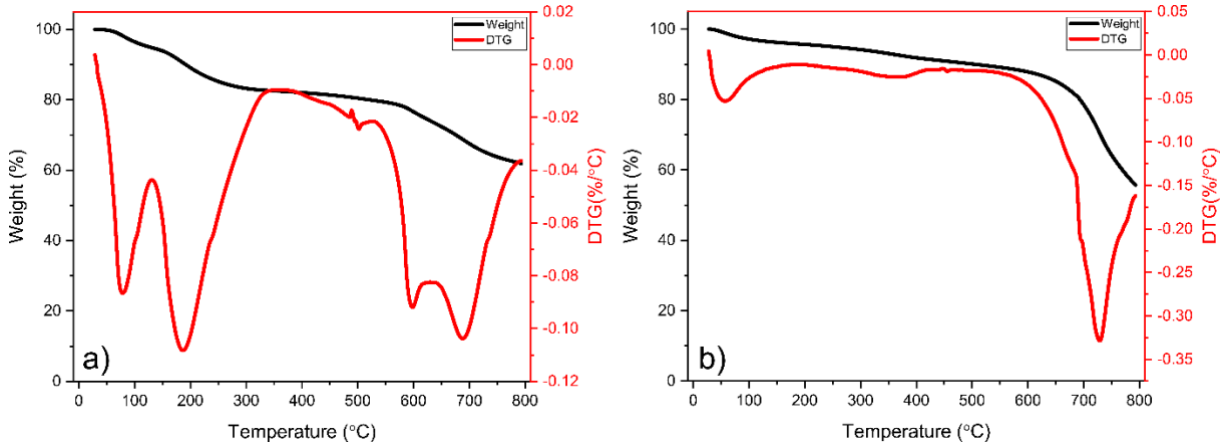

Fig. 3 Weight (%) and DTG (%/°C) analyses of a) neat PBI nanofibers and b) heat-treated PBI nanofibers (DTG, Derivative thermogravimetric).

3.2 Structural Optimization of CNTs/PBI Nanocarpets

CNT synthesis on the PBI nanofiber substrates was accomplished using CVD method. The operating temperature inside the quartz tube was controlled to be 600 °C since the primary decomposition takes place around 700 °C as shown in Fig. 3. After removal of LiCl stabilizer, the weight change of the PBI substrate remains between 5-10% till the 600 °C defined as growth temperature. Anchoring CNTs on PBI nanofibers enables direct CNT growth while causing little to no damage on the nanofibrous substrate as the operating temperature does not exceed the degradation temperature of PBI nanofibers. Nevertheless, the time and temperature cycles both in the nucleation and growth stages were required to be monitored to address their effect on the structural and physical characteristics of grown CNTs.

Table 1 describes the parametric exploration of the nucleation and growth stages in the CVD process. Based on the nucleation and growth times, the samples were coded in the following manner: The sample subjected to 10 min of nucleation step and 15 min of growth step with 1 mM catalyst concentration was named as M1N10G15, where M, N, and G denote the molarity of the catalyst, the nucleation and growth times, respectively. In this study, M was decided to be either 1 or 10 mM while N and G were chosen as 10 or 15 min, resulting in a total of 8 samples.

Table 1 The parametric nucleation and growth times for the CNT growth on the PBI nanofibers.

Sample (1 or 10 mM)	Nucleation Time (min)	Growth Time (min)
N10G10	10	10
N10G15	10	15
N15G10	15	10
N15G15	15	15

3.2 Morphology of CNTs/PBI Nanocarpets

Curved nanofibers would behave differently than smooth surfaces and micron-sized fibers due to having nanoscopic features, thus provide different assistance to the CNT growth. To reveal the effect of roughness and curvature of the substrate on the alignment of CNTs, we also used a commercial PBI smooth polymeric film (Fumatech AM-30) as a reference and then catalyzed it with 10 mM precursor catalyst solution. Following the aforementioned CVD process with nucleation and growth times of 15 and 10 min, respectively, CNT synthesis was achieved. The cross-sectional SEM images revealed

uniform growth on the smooth surface and they are provided in the Supplementary Information (Fig. S2). Furthermore, the mean CNT diameter and the array length were measured using an image processing tool, ImageJ software, as 71±10 nm and 0.7±0.1 μm, respectively. This exploration validated the proposed CNT growth methodology using PBI based polymeric substrates. Nevertheless, we tuned the growth procedure while introducing PBI nanofibrous substrates along with a process optimization, aiming an optimal CNT coverage and uniformity.

Employing heterogenous PBI nanofibrous substrate resulted in considerable structural differences in CNT growth coupled with nucleation and growth process parameters. Therefore, unraveling the effect of CVD process parameters is crucial for tuning the structural characteristics and the microstructure of the grown CNTs. The SEM images of each sample and their close-up insets are shown in Fig. 4. The morphology analysis revealed the dependency of CNTs physical properties, and the boundaries in terms of to what extent by tuning the process to achieve dense, long and relatively aligned arrays.

Fig. 4a and 4b demonstrate that the CNT growth was hindered in both M1N10G10 and M10N10G10 samples where possibly the surface of the nanofibers was not coated completely, in other words insufficient number of nucleation sites was created due to less exposure to the nucleating gas of H_2 during the nucleation stage [40]. Fig. 4c and 4d point out that better coverage of CNT arrays was achieved when carbon source gas was flushed for an extra 5 min during the growth stage. In other words, as C_2H_4 continued to flow inside the chamber during the growth stage, the intensity of the grown CNTs increased regardless of the catalyst concentration. However, a full-coverage of the fibers was not achieved as barren zones on the nanofibers were observed for both M1N10G15 and M10N10G15 samples. This behavior could be attributed to the low density of nucleation sites leading to non-uniform surface morphology, as noted by Yamamoto et al. [40]. Furthermore, increasing the nucleation time to 15 min resulted in better coverage on the surface of the nanofibers due to denser nucleation sites, as interpreted from Fig. 4e-h, re-emphasizing the importance of H_2 pre-treatment [43]. The effect of increasing the growth time from 10 min to 15 min which could be followed in Fig. 4e to 4g and Fig. 4f to 4h, caused highly dense CNT arrays, indicating better coverage due to grown CNTs.

Investigation of the morphology of the samples led to the plain fact that was the nucleation time or H_2 pre-treatment being the most prominent parameter in CNT growth regardless of the catalyst concentration and growth time. Longer nucleation time (i.e., 15 min) resulted in higher CNT density

for the cases of N15G10 and N15G15, as shown in Fig. 4e-h. Besides, the length of the CNT arrays was also found to be increasing with elongated nucleation times as it caused more uniform coating of nanofibers, leading to longer CNT arrays regardless of the catalyst concentration (~65% and ~190% increases for 1 and 10 mM). In addition to nucleation time, growth time also played a positive role in the morphology of CNTs. It is an expected behavior to observe more extended CNT arrays with increased exposure time to carbon source gas during the growth process [54]. Even though the CNT array lengths raised in both cases, the variation in the case of 1 mM catalyst concentration was found to be small (~8%) while the outcome in 10 mM case was substantial (~55%). This trend could be explained by the coating of nanofibers, pointing out another critical parameter: catalyst concentration.

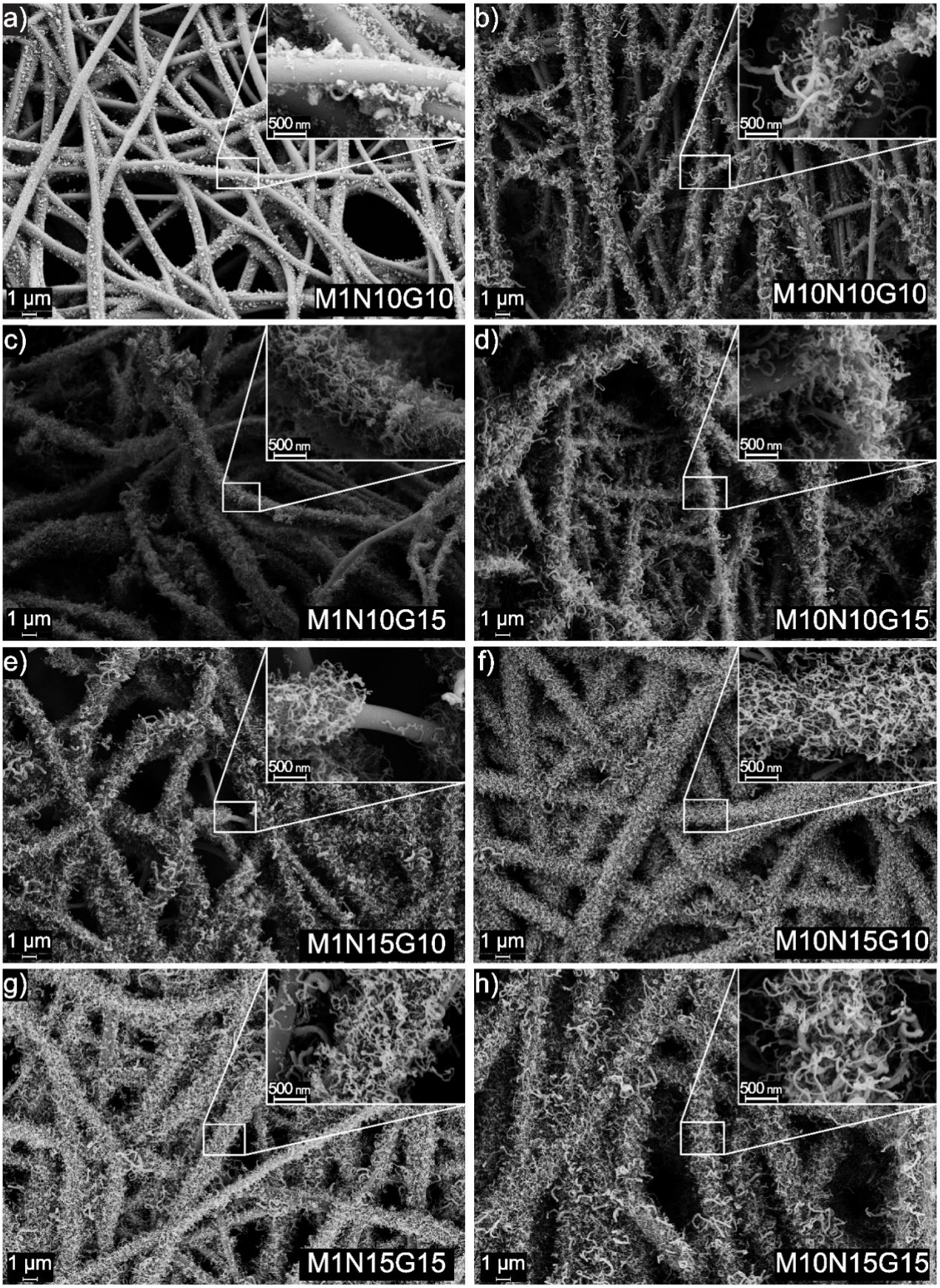

Fig. 4 SEM micrographs of a) M1N10G10, b) M10N10G10, c) M1N10G15, d) M10N10G15, e) M1N15G10, f) M10N15G10, g) M1N15G15, and h) M10N15G15 where inset images reveal the orientation and volumetric distribution of CNTs on curved PBI nanofibers.

Higher catalyst concentrations facilitated more active sites on the nanofibers, thus leading to considerably higher intensity of CNT forests. When the surface of the nanofibers was activated with adequate catalyst sites, the vast number of grown CNTs created crowding effect as the neighboring CNTs force adjacent ones to grow up in a straighter route [48]. Accordingly, regarding the alignment of the CNTs, this effect played an important role in orientation. As a result, the CNTs grew longer and radially oriented in the samples doped with 10 mM catalyst as it granted a high amount of nucleation sites for CNT growth. However, extended growth times (i.e., 15 min) resulted in even longer CNT arrays, and eventually, they became bent and tangled, a characteristic expression noted by Hou et al. [54]. Particularly, the nanotubes observed in Fig. 4g-h are quite similar to the ones reported by Hou et al. demonstrating bent and tangled CNT structure. Although CVD parameters were critically affecting the morphology of the CNTs/PBI samples, the mean CNT diameters have not correlated either with the nucleation or growth times [18].

A closer look into the inset images quantified the physical properties of CNTs such as the array lengths, measured from 30 to 40 different locations in each case. Since the grown CNTs provide coverage around the nanofibers, the mean array length of the grown CNTs was determined by subtracting the diameter of the nanofibers from the total array length and dividing it by two, as depicted in the Supplementary Information (Fig. S3). The mean array length and mean diameter of CNTs are summarized in Table 2. Due to inconsistent CNT coverage in M1N10G10 and M10N10G10 samples, the mean array length could not be adequately measured. Tuning the process parameters, the nucleation and growth times were found to be directly affecting the CNT array lengths of the samples.

Table 2 Mean CNT diameters and array lengths measured on CNTs/PBI nanocarpets.

		N10G10	N10G15	N15G10	N15G15
Diameter (nm)	1 mM	23.5±3.0	24.0±4.3	27.1±4.3	24.5±4.4
	10 mM	38.7±9.4	30.3±7.6	27.2±3.8	28.2±5.6
Array Length (μm)	1 mM	N/A	0.306±0.047	0.474±0.062	0.508±0.121
	10 mM	N/A	0.277±0.066	0.518±0.083	0.805±0.073

Judging by the SEM images, the highest quality samples in terms of uniform coverage and radial alignment were identified as M10N15G10 and M10N15G15. Therefore, TEM analyses were conducted on these select samples to quantify the grown CNTs, including the number of walls and wall thickness. Fig. 5a-b proves the existence of CNTs while highlighting the multi-walled nanotube assemblies. The number of walls was found to be in the range of 20-45 and 21-25 for M10N15G10

and M10N15G15, respectively. The mean outer diameters of CNTs were measured to be 26.46±10.56 nm and 34.30±6.50 nm for M10N15G10 and M10N15G15 samples, respectively. Furthermore, Fig. 5c-d revealed that Fe^{3+} nanoparticles were found at the tip of CNTs in an encapsulated form, diameters of which were consistent with that of CNTs, indicating the tip-growth CNT formation on PBI nanofiber where weak interaction between the substrate and the catalyst was formed.

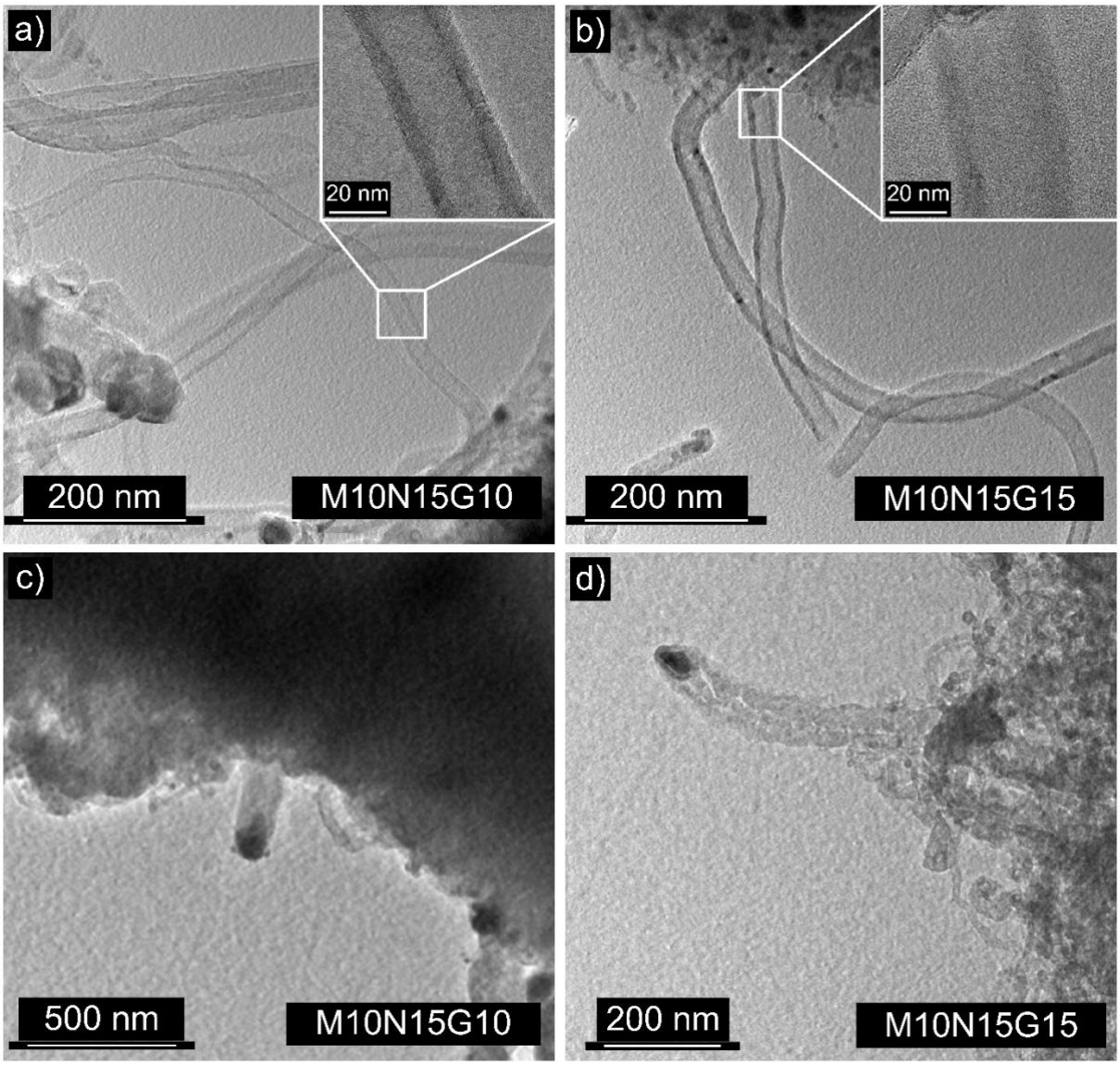

Fig. 5 TEM images of CNTs/PBI nanocarpets where insets showing individual CNTs revealing multi-walled graphitic structures: a) M10N15G10 and b) M10N15G15; and TEM images showing tip growth of CNTs on PBI nanofibers: c) M10N15G10 and d) M10N15G15.

The Raman spectroscopy was used to analyze the quality of the grown CNTs with different catalyst concentrations and various nucleation and growth times. The Raman spectroscopy results shown in the Supplementary Material (Fig. S4) demonstrated two distinct peaks, G peak seen at 1593 cm^{-1}, which was attributed to the in-plane vibrations of sp^2 bonded atoms and D peak seen at 1344 cm^{-1} resulting from the out-of-plane vibrations of sp^3 bonded atoms, expressing the structural defects of

carbon atoms. The higher intensity in D peaks indicates more defects and more significant number of broken sp^2 bonded atoms [55]. Typically, I_g/I_d ratio is a quite useful measure to determine the structural quality of the grown CNTs. Therefore, I_g/I_d ratios were calculated from Fig. S4 to evaluate the quality of the grown CNTs on PBI nanofibers.

The quality of the grown CNTs was found to be quite similar in each case. Therefore, when working with heterogeneous substrates, it can be deduced that there was no strong dependency between the CNT quality and the parameters examined in this study. A slight deviation in the CNT quality was believed to be resulting from the nucleation time. As the nucleation time was increased from 10 min to 15 min, a negligible decline in the I_g/I_d ratio was observed. This behavior could be attributed to the increase in the accumulated iron catalyst, which leads to a loss of crystallinity of CNTs.

Intensity, packing density and the alignment of the CNT forests on the substrates are the most prominent parameters affecting electrical conductivity [56,57]. The quality and the number of CNTs have an impact on the efficiency of the electron transfer through the nanofiber network. The electrical conductivity of each sample was measured using a four-point probe and the results are depicted in Fig. 6. The electrical conductivities of the samples doped with 1 mM catalyst were insensitive to changes in nucleation and growth times and displayed a similar conductivity profile except for the M1N15G15 sample. When the catalyst molarity was increased to 10 mM, the electron conduction mechanism became very sensitive to variations in the nucleation and growth times. The highest electrical conductivity was obtained as 0.039±0.004 S/cm with the M10N15G15 sample.

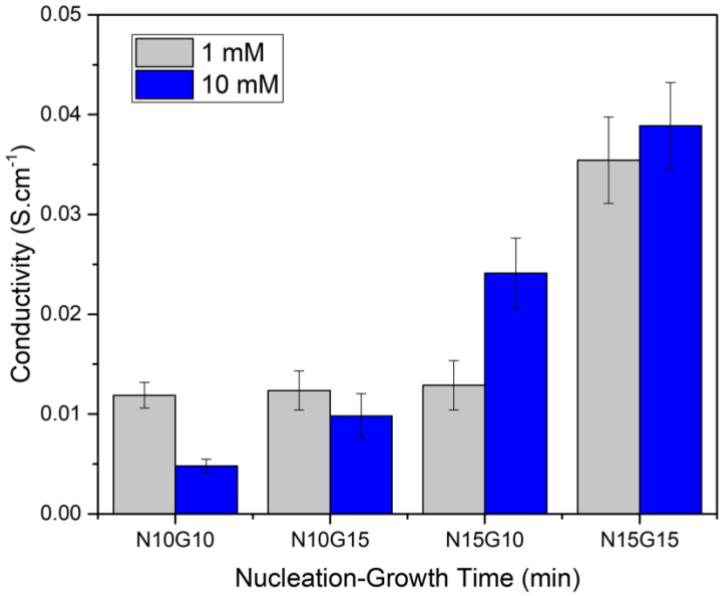

Fig. 6 The four-point electrical conductivity of CNTs/PBI nanocarpets revealing the effect of catalyst concentrations at different nucleation and growth times.

The electrical conductivity results revealed that N15G15 samples with both catalyst concentrations yielded the highest surface conductivities, which was strongly attributed to the volumetric intensity of CNT forests. A similar behavior, an increase in the electrical conductivity due to augmented CNTs buckypaper density was reported by Chen et al. [56]. Since the CNTs in each sample did not manifest a notable difference in terms of diameter, the increase in the electrical conductivity could be explained with the improved array lengths. Hence, more effective electron conduction paths were generated for the samples with more extended CNT arrays, boosting the electrical conductivity of M1N15G15, M10N15G10, and M10N15G15 samples [39].

4. Conclusions

Direct growth of CNTs on the electrospun polymeric nanofibrous mats was successfully carried out by the CVD method. Uniform coverage and conformance of CNTs on the PBI nanofibers were achieved by conducting a series of parametric experiments, alternating the catalyst concentration and the nucleation and growth times, under a fixed CVD furnace temperature of 600 °C. The results indicated that the suggested pathway enabled successful growth of CNTs on nanofibrous mats without damaging the substrate significantly. The synthesized CNTs grown on PBI nanofibers possessed the potential of serving as interleaves in lithium batteries and structural composites, benefiting from the synergetic effect of PBI nanofiber scaffold and stiff CNTs to enhance electrical properties of the overall structure, achieving electrical conductivity values as high as 0.039±0.004 S/cm with CVD parameters of 10 mM catalyst concentration and 15 min of nucleation and growth times.

Acknowledgments

This research was funded by TUBITAK (The Scientific and Technological Research Council of Turkey) under the career development R&D Projects funding program with a grant number 116M427. The authors would like to thank Mr. Firat Turgut for his assistance on the optimization of CVD process and Dr. Ozgur Duygulu from TUBITAK MAM for his efforts in the TEM analysis.

CRediT authorship contribution statement

Kaan Yildiz: Conceptualization, Methodology, Writing – review & editing. **Adel Alrai:** Investigation, Formal analysis, methodology. **Melike Erturk:** Investigation, methodology. **Deniz Koken:** Investigation, Formal analysis. **Beyza Bozali:** Writing – original draft, Methodology, Visualization. **Afshin Zamani Zakaria:** Writing – original draft, Methodology, Visualization. **Fevzi Cakmak Cebeci:** Supervision. **Elif Ozden-Yenigun:** Conceptualization, Writing – review & editing,

Supervision, Project administration. **Hulya Cebeci:** Conceptualization, Writing – review & editing, Supervision, Project administration.

Conflicts of interest

There are no conflicts to declare.

Data availability

The data presented in this study are available on request from the corresponding author.

Supplementary information

Supplementary information related to this article can be found in the online version.

Ethical approval

No ethical approval was required for this research as it did not involve human tissue or any other parts of living organisms.

References:

[1] Qian, H., Greenhalgh, E. S., Shaffer, M. S., and Bismarck, A. "Carbon Nanotube-Based Hierarchical Composites: A Review." Journal of Materials Chemistry, Vol. 20, No. 23, 2010, pp. 4751–4762.

[2] Su, Y.-S., and Manthiram, A. "A New Approach to Improve Cycle Performance of Rechargeable Lithium--Sulfur Batteries by Inserting a Free-Standing MWCNT Interlayer." Chemical Communications, Vol. 48, No. 70, 2012, pp. 8817–8819.

[3] Jun, J. H., Song, H., and Jeong, Y. "Ultra-Lightweight and Flexible Current Collector Based on Freestanding Carbon Nanotube Sheets for Lithium-Ion Capacitors." *Advanced Materials Technologies*, Vol. 4, No. 2, 2019, p. 1800452.

[4] Deng, S., Zhang, Q., Huang, Q., Tang, D., Mei, P., and Yang, Y. "Carbon Nanotube-Supported Polyimide Nanoarrays as Sulfur Host with Physical/Chemical Polysulfide-Traps for Li--S Batteries." *Composites Communications*, 2021, p. 101019.

[5] Lee, J. S., Jun, J., Cho, S., Kim, W., and Jang, J. "Electrospun Three-Layered Polymer Nanofiber-Based Porous Carbon Nanotubes for High-Capacity Energy Storage." *RSC Advances*, Vol. 7, No. 1, 2017, pp. 201–207.

[6] Cai, M., Sun, X., Chen, W., Qiu, Z., Chen, L., Li, X., Wang, J., Liu, Z., and Nie, Y. "Performance of Lithium-Ion Capacitors Using Pre-Lithiated Multiwalled Carbon Nanotubes/Graphite Composite as Negative Electrode." *Journal of Materials Science*, Vol. 53, No. 1, 2018, pp. 749–758. https://doi.org/10.1007/s10853-017-1524-5.

[7] Zhang, Y., Li, K., Ji, P., Chen, D., Zeng, J., Sun, Y., Zhang, P., and Zhao, J. "Silicon-Multi-Walled Carbon Nanotubes-Carbon Microspherical Composite as High-Performance Anode for

Lithium-Ion Batteries." *Journal of Materials Science*, Vol. 52, No. 7, 2017, pp. 3630–3641. https://doi.org/10.1007/s10853-016-0503-6.

[8] Lv, P., Feng, Y., Zhang, P., Chen, H., Zhao, N., and Feng, W. "Increasing the Interfacial Strength in Carbon Fiber/Epoxy Composites by Controlling the Orientation and Length of Carbon Nanotubes Grown on the Fibers." *Carbon*, Vol. 49, No. 14, 2011, pp. 4665–4673.

[9] Johnson, R. J., Tang, J., and Pitchumani, R. "Characterization of Damping in Carbon-Nanotube Filled Fiberglass Reinforced Thermosetting-Matrix Composites." *Journal of Materials Science*, Vol. 46, No. 13, 2011, pp. 4545–4554. https://doi.org/10.1007/s10853-011-5349-3.

[10] Shen, X., Jia, J., Chen, C., Li, Y., and Kim, J.-K. "Enhancement of Mechanical Properties of Natural Fiber Composites via Carbon Nanotube Addition." *Journal of Materials Science*, Vol. 49, No. 8, 2014, pp. 3225–3233. https://doi.org/10.1007/s10853-014-8027-4.

[11] Piloto, C., Mirri, F., Bengio, E. A., Notarianni, M., Gupta, B., Shafiei, M., Pasquali, M., and Motta, N. "Room Temperature Gas Sensing Properties of Ultrathin Carbon Nanotube Films by Surfactant-Free Dip Coating." *Sensors and Actuators B: Chemical*, Vol. 227, 2016, pp. 128–134.

[12] Zhang, Q., Liu, J., Sager, R., Dai, L., and Baur, J. "Hierarchical Composites of Carbon Nanotubes on Carbon Fiber: Influence of Growth Condition on Fiber Tensile Properties." *Composites Science and Technology*, Vol. 69, No. 5, 2009, pp. 594–601.

[13] Allen, A., Cannon, A., Lee, J., King, W. P., and Graham, S. "Flexible Microdevices Based on Carbon Nanotubes." *Journal of Micromechanics and Microengineering*, Vol. 16, No. 12, 2006, p. 2722.

[14] Tsotsis, T. K. "Interlayer Toughening of Composite Materials." *Polymer Composites*, Vol. 30, No. 1, 2009, pp. 70–86.

[15] Chen, J., Liu, B., Gao, X., and Xu, D. "A Review of the Interfacial Characteristics of Polymer Nanocomposites Containing Carbon Nanotubes." *RSC Advances*, Vol. 8, No. 49, 2018, pp. 28048–28085.

[16] Veedu, V. P., Cao, A., Li, X., Ma, K., Soldano, C., Kar, S., Ajayan, P. M., and Ghasemi-Nejhad, M. N. "Multifunctional Composites Using Reinforced Laminae with Carbon-Nanotube Forests." *Nature Materials*, Vol. 5, No. 6, 2006, pp. 457–462. https://doi.org/10.1038/nmat1650.

[17] Ghasemi, N. M. N., P, V. V., Anyuan, C., Pulickel, A., and Davood, A. Three-Dimensionally Reinforced Multifunctional Nanocomposites, *U.S. Patent No. 8,148,276*. Washington, DC: U.S. Patent and Trademark Office, 2012.

[18] Liu, K., Sun, Y., Chen, L., Feng, C., Feng, X., Jiang, K., Zhao, Y., and Fan, S. "Controlled Growth of Super-Aligned Carbon Nanotube Arrays for Spinning Continuous Unidirectional Sheets with Tunable Physical Properties." *Nano Letters*, Vol. 8, No. 2, 2008, pp. 700–705.

[19] Agnihotri, P., Basu, S., and Kar, K. “Effect of Carbon Nanotube Length and Density on the Properties of Carbon Nanotube-Coated Carbon Fiber/Polyester Composites.” *Carbon*, Vol. 49, No. 9, 2011, pp. 3098–3106.

[20] Inoue, Y., Suzuki, Y., Minami, Y., Muramatsu, J., Shimamura, Y., Suzuki, K., Ghemes, A., Okada, M., Sakakibara, S., Mimura, H., and Naito, K. “Anisotropic Carbon Nanotube Papers Fabricated from Multiwalled Carbon Nanotube Webs.” *Carbon*, Vol. 49, No. 7, 2011, pp. 2437–2443. https://doi.org/10.1016/j.carbon.2011.02.010.

[21] Cheng, H., Dong, Z., Hu, C., Zhao, Y., Hu, Y., Qu, L., Chen, N., and Dai, L. “Textile Electrodes Woven by Carbon Nanotube--Graphene Hybrid Fibers for Flexible Electrochemical Capacitors.” *Nanoscale*, Vol. 5, No. 8, 2013, pp. 3428–3434.

[22] Guo, F., Kang, T., Liu, Z., Tong, B., Guo, L., Wang, Y., Liu, C., Chen, X., Zhao, Y., Shen, Y., and others. “Advanced Lithium Metal--Carbon Nanotube Composite Anode for High-Performance Lithium--Oxygen Batteries.” *Nano Letters*, Vol. 19, No. 9, 2019, pp. 6377–6384.

[23] Gao, F., Mei, B., Xu, X., Ren, J., Zhao, D., Zhang, Z., Wang, Z., Wu, Y., Liu, X., and Zhang, Y. “Rational Design of ZnMn2O4 Nanoparticles on Carbon Nanotubes for High-Rate and Durable Aqueous Zinc-Ion Batteries.” *Chemical Engineering Journal*, Vol. 448, 2022, p. 137742.

[24] Badatya, S., Bharti, D. K., Sathish, N., Srivastava, A. K., and Gupta, M. K. “Humidity Sustainable Hydrophobic Poly (Vinylidene Fluoride)-Carbon Nanotubes Foam Based Piezoelectric Nanogenerator.” *ACS Applied Materials & Interfaces*, Vol. 13, No. 23, 2021, pp. 27245–27254.

[25] Li, P., Wang, C., Zhang, Y., and Wei, F. “Air Filtration in the Free Molecular Flow Regime: A Review of High-Efficiency Particulate Air Filters Based on Carbon Nanotubes.” *Small*, Vol. 10, No. 22, 2014, pp. 4543–4561.

[26] Bilge, K., Ozden-Yenigun, E., Simsek, E., Menceloglu, Y., and Papila, M. “Structural Composites Hybridized with Epoxy Compatible Polymer/MWCNT Nanofibrous Interlayers.” *Composites Science and Technology*, Vol. 72, No. 14, 2012, pp. 1639–1645.

[27] Ozden-Yenigun, E., Atilgan, C., and Elliott, J. A. “Multi-Scale Modelling of Carbon Nanotube Reinforced Crosslinked Interfaces.” *Computational Materials Science*, Vol. 129, 2017, pp. 279–289.

[28] Song, X., Gao, J., Zheng, N., Zhou, H., and Mai, Y.-W. “Interlaminar Toughening in Carbon Fiber/Epoxy Composites Interleaved with CNT-Decorated Polycaprolactone Nanofibers.” *Composites Communications*, Vol. 24, 2021, p. 100622.

[29] Askari, D., and Ghasemi-Nejhad, M. N. “Effects of Vertically Aligned Carbon Nanotubes on Shear Performance of Laminated Nanocomposite Bonded Joints.” *Science and Technology of Advanced Materials*, Vol. 13, No. 4, 2012, p. 045002. https://doi.org/10.1088/1468-6996/13/4/045002.

[30] Singhal, R., Chung, S.-H., Manthiram, A., and Kalra, V. “A Free-Standing Carbon Nanofiber Interlayer for High-Performance Lithium--Sulfur Batteries.” *Journal of Materials Chemistry A*, Vol. 3, No. 8, 2015, pp. 4530–4538.

[31] Yang, T., and Chung, T.-S. “High Performance ZIF-8/PBI Nano-Composite Membranes for High Temperature Hydrogen Separation Consisting of Carbon Monoxide and Water Vapor.” *International Journal of Hydrogen Energy*, Vol. 38, No. 1, 2013, pp. 229–239.

[32] Olagoke, O., and Adewale, K. *Handbook of Thermoplastics*. CRC press, 2016.

[33] Jahangiri, S., Aravi, İ., Şanlı, L. I., Menceloğlu, Y. Z., and Özden-Yenigün, E. “Fabrication and Optimization of Proton Conductive Polybenzimidazole Electrospun Nanofiber Membranes.” *Polymers for Advanced Technologies*, Vol. 29, No. 1, 2018, pp. 594–602.

[34] Kim, J.-S., and Reneker, D. H. “Polybenzimidazole Nanofiber Produced by Electrospinning.” *Polymer Engineering & Science*, Vol. 39, No. 5, 1999, pp. 849–854.

[35] Dzenis, Y. A., and Reneker, D. H. Delamination Resistant Composites Prepared by Small Diameter Fiber Reinforcement at Ply Interfaces, , 2001.

[36] Kannan, R., Kagalwala, H. N., Chaudhari, H. D., Kharul, U. K., Kurungot, S., and Pillai, V. K. “Improved Performance of Phosphonated Carbon Nanotube--Polybenzimidazole Composite Membranes in Proton Exchange Membrane Fuel Cells.” *Journal of Materials Chemistry*, Vol. 21, No. 20, 2011, pp. 7223–7231.

[37] Li, H.-Y., and Liu, Y.-L. “Polyelectrolyte Composite Membranes of Polybenzimidazole and Crosslinked Polybenzimidazole-Polybenzoxazine Electrospun Nanofibers for Proton Exchange Membrane Fuel Cells.” *Journal of Materials Chemistry A*, Vol. 1, No. 4, 2013, pp. 1171–1178.

[38] Kumar, M. Carbon Nanotube Synthesis and Growth Mechanism. In *Carbon Nanotubes - Synthesis, Characterization, Applications* (S. Yellampalli, ed.), InTech, Rijeka, Croatia, 2011, pp. 147–170.

[39] Wang, X., Jiang, Q., Xu, W., Cai, W., Inoue, Y., and Zhu, Y. “Effect of Carbon Nanotube Length on Thermal, Electrical and Mechanical Properties of CNT/Bismaleimide Composites.” *Carbon*, Vol. 53, 2013, pp. 145–152.

[40] Yamamoto, N., Hart, A. J., Garcia, E. J., Wicks, S. S., Duong, H. M., Slocum, A. H., and Wardle, B. L. “High-Yield Growth and Morphology Control of Aligned Carbon Nanotubes on Ceramic Fibers for Multifunctional Enhancement of Structural Composites.” *Carbon*, Vol. 47, No. 3, 2009, pp. 551–560.

[41] Lee, Y. T., Park, J., Choi, Y. S., Ryu, H., and Lee, H. J. “Temperature-Dependent Growth of Vertically Aligned Carbon Nanotubes in the Range 800- 1100 C.” *The Journal of Physical Chemistry B*, Vol. 106, No. 31, 2002, pp. 7614–7618.

[42] Jo, S., Wang, D., Huang, J., Li, W., Kempa, K., and Ren, Z. “Field Emission of Carbon Nanotubes Grown on Carbon Cloth.” *Applied Physics Letters*, Vol. 85, No. 5, 2004, pp. 810–812.

[43] Singh, C., Shaffer, M. S., and Windle, A. H. “Production of Controlled Architectures of Aligned Carbon Nanotubes by an Injection Chemical Vapour Deposition Method.” *Carbon*, Vol. 41, No. 2, 2003, pp. 359–368.

[44] Wang, Y., Zhang, K., Zou, J., Wang, X., Sun, L., Wang, T., and Zhang, Q. “Functionalized Horizontally Aligned CNT Array and Random CNT Network for CO2 Sensing.” *Carbon*, Vol. 117, 2017, pp. 263–270.

[45] Handuja, S., Srivastava, P., and Vankar, V. “On the Growth and Microstructure of Carbon Nanotubes Grown by Thermal Chemical Vapor Deposition.” *Nanoscale Research Letters*, Vol. 5, No. 7, 2010, pp. 1211–1216.

[46] Afre, R. A., Soga, T., Jimbo, T., Kumar, M., Ando, Y., and Sharon, M. “Growth of Vertically Aligned Carbon Nanotubes on Silicon and Quartz Substrate by Spray Pyrolysis of a Natural Precursor: Turpentine Oil.” *Chemical Physics Letters*, Vol. 414, Nos. 1–3, 2005, pp. 6–10.

[47] Yamada, T., Namai, T., Hata, K., Futaba, D. N., Mizuno, K., Fan, J., Yudasaka, M., Yumura, M., and Iijima, S. “Size-Selective Growth of Double-Walled Carbon Nanotube Forests from Engineered Iron Catalysts.” *Nature Nanotechnology*, Vol. 1, No. 2, 2006, pp. 131–136.

[48] Xu, M., Futaba, D. N., Yumura, M., and Hata, K. “Alignment Control of Carbon Nanotube Forest from Random to Nearly Perfectly Aligned by Utilizing the Crowding Effect.” *ACS Nano*, Vol. 6, No. 7, 2012, pp. 5837–5844.

[49] Özden-Yenigün, E., Bilge, K., Sünbüloğlu, E., Bozdağ, E., and Papila, M. “High Strain Rate Response of Nanofiber Interlayered Structural Composites.” *Composite Structures*, Vol. 168, 2017, pp. 47–55.

[50] Rabbani, A., and Salehi, S. “Dynamic Modeling of the Formation Damage and Mud Cake Deposition Using Filtration Theories Coupled with SEM Image Processing.” *Journal of Natural Gas Science and Engineering*, Vol. 42, 2017, pp. 157–168. https://doi.org/10.1016/j.jngse.2017.02.047.

[51] Ezeakacha, C. P., Rabbani, A., Salehi, S., and Ghalambor, A. “Integrated Image Processing and Computational Techniques to Characterize Formation Damage.” *Day 1 Wed, February 07, 2018*, 2018. https://doi.org/10.2118/189509-ms.

[52] PBI Performance Products, Polybenzimidazole (PBI) S26 Solution. https://pbipolymer.com/wp-content/uploads/2016/05/Celazole-PBI-S26-Typical-Properties.pdf.

[53] Dinari, M., Nabiyan, A., Ensafi, A. A., and Jafari-Asl, M. “Polybenzimidazole and Polybenzimidazole/MoS 2 Hybrids as an Active Nitrogen Sites: Hydrogen Generation Application.” *RSC Advances*, Vol. 5, No. 122, 2015, pp. 100996–101005.

[54] Hou, H., and Reneker, D. H. "Carbon Nanotubes on Carbon Nanofibers: A Novel Structure Based on Electrospun Polymer Nanofibers." *Advanced Materials*, Vol. 16, No. 1, 2004, pp. 69–73.

[55] Herrero-Latorre, C., Álvarez-Méndez, J., Barciela-García, J., García-Martín, S., and Peña-Crecente, R. "Characterization of Carbon Nanotubes and Analytical Methods for Their Determination in Environmental and Biological Samples: A Review." *Analytica Chimica Acta*, Vol. 853, 2015, pp. 77–94.

[56] Chen, G., Futaba, D. N., Sakurai, S., Yumura, M., and Hata, K. "Interplay of Wall Number and Diameter on the Electrical Conductivity of Carbon Nanotube Thin Films." *Carbon*, Vol. 67, 2014, pp. 318–325.

[57] Zhang, L., Zhang, G., Liu, C., and Fan, S. "High-Density Carbon Nanotube Buckypapers with Superior Transport and Mechanical Properties." *Nano Letters*, Vol. 12, No. 9, 2012, pp. 4848–4852.